Experimental Mechanics (2007) 47:373–380
DOI 10.1007/s11340-006-9014-8

Measurement of Deformation and Strain in Nitinol

K.E. Perry · P.E. Labossiere · E. Steffler

Received: 20 June 2006 / Accepted: 11 October 2006 / Published online: 15 February 2007

Abstract Phase shifted moiré interferometry is used to measure full-field strains during uniaxial tension and four-point bend loading of nitinol test samples. Optical resolution and grating coherence were exceptional and allowed simultaneous resolution of the strain fields within both the parent and transformed phases of the material. Evidence of localized and uniformly distributed phase transformation was observed for the samples tested in uniaxial tension while the bending results indicate a clear tension/compression asymmetry. The results further highlight the effect of the elasticity of the two phases and the complexity associated with competing martensite and R-phase transformations on the thermomechanical behavior of nitinol. Finally, the technique is applied to a nitinol implantable medical component to demonstrate the opportunities for improved end-use material characterization, numerical modeling and design validation.

Keywords Nitinol · Thermoelasticity · Phase transformations · Photomechanics · Moiré interferometry · Full-field measurements · Modeling · Carrier fringes

K.E. Perry (✉, SEM member) · P.E. Labossiere
ECHOBIO LLC, 579 Azalea Avenue, Bainbridge Island, WA 98110, USA
e-mail: kperry@echobio.com

E. Steffler
Idaho National Engineering Laboratory, Idaho Falls, ID 83415, USA

Introduction

Nitinol has seen increased use in medical applications where devices are compressed to catheter dimensions, delivered through tortuous anatomy and deployed in various diseased locations within the human body. The material is well suited to the design constraints imposed by such conditions and often provides incomparable advantages over other engineering materials. Alloy composition and processing history [1–3] can be used to achieve a broad range of material response that can be tailored to intended applications.

The deformation behavior of nitinol is complicated by a number of factors attributed to the materials unique multi-phase composition. Tension/compression asymmetry, phase boundary localization, loading and temperature history all contribute to the complexity of the observed deformation response of nitinol.

Recent studies by the authors have demonstrated the application of phase shifted moiré interferometry [4] to strain measurements in nitinol [5] with special attention to experimental details such as the effect of specimen grating thickness and density, fringe analysis and the quantification of full-field and real-time strains [6]. For our work, we exploit phase shifting [7] which provides exceptional noise reduction while enhancing spatial resolution and enabling real-time (video frame rate) data analysis.

For this work we utilize a novel nitinol coupon sample geometry [8] that is used to study both uniaxial tension and four point bending deformation over a range of temperatures both above and below the A_f temperature for materials with well characterized heat treatment histories. Measurements of two-way shape memory and an application of the technique to a typical

medical device are included to further illustrate the opportunities for developing improved test methods and design tools for implantable nitinol components.

Experiment

Material, Processing History and Test Sample

The material used in this study was SE-508, seamless drawn tubing from Nitinol Devices and Components, Inc. with an as-received A_f of −9°C. At temperatures above the A_f, or austenite finishing temperature, only the austenite phase of the material is present. Similarly, below the M_f, or martensite finishing temperature, the sample consists of only the martensite phase. Additional phases are typically present, such as the R-phase, similarly characterized by R'_f.

Two distinct heat treatments were chosen, denoted by A and B. Treatment A was performed at 325°C for 60 min and treatment B was performed at 500°C for 30 min. All samples were water quenched subsequent to heat treating.

The active A_f temperatures were measured for all test samples following ASTM standard F-2082 for free bend and recovery over the temperature range from −30 to 30°C. Very consistent results were obtained and details have been presented elsewhere [8]. Treatment A resulted in test samples with an active A_f of 25.4°C and exhibited a strong R-phase component with an R'_f of −3.5°C. Treatment B did not exhibit a noticeable R-phase component and had an active A_f of 22°C.

A single sample geometry was chosen for both uniaxial tension and four-point bending tests. Figure 1 is a schematic of the sample geometry and photographs of the two loading scenarios.

Two pairs of holes were laser cut in the ends of the samples and then carefully honed to insure precision pin loading of the test samples. The gage section of the samples were EDM'ed to produce perpendicular edges, maximizing the amount of material in the gage section and ensuring uniform behavior in bending. Slow feed, low power and multiple passes were used to minimize adverse effects on the bulk material properties. A flat surface was carefully ground on one face of the test samples to provide an optically flat surface for the grating replication process. Prior to production of the samples, FEA was used to optimize the design of the sample geometry and the corresponding fixtures to achieve uniform tension and pure bending over a large range of deformations. A slow loading rate (<1 mm/min) was used for all of the tests.

Loading and Global Data Measurements

The samples were loaded in either tension or bending using a custom built load frame and fixtures. Global (Far-field) measurements of the sample load, extension and displacement were made using a load cell, extensometer with a gage length of 10 mm and LVDT, respectively.

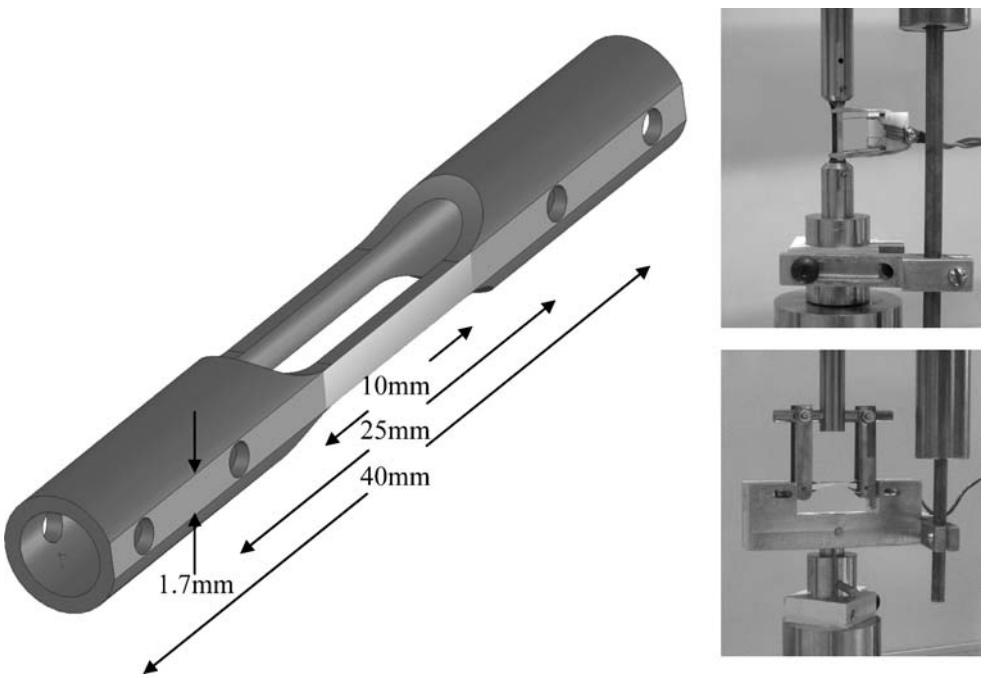

Fig. 1 Schematic of the test sample and photographs of the tensile and four-point bend configurations

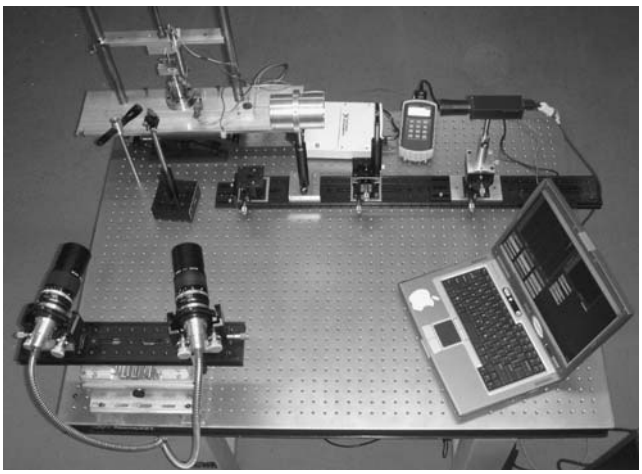

Fig. 2 Photograph of the custom load frame and two beams of the fiber optic moiré interferometer

A minimum of two thermocouples were used to monitor temperature of the samples during the experiments. A laminar flow of chilled or warmed dry air was directed over the sample to provide temperature control over a range of −20–40°C. The sample temperatures were held within 1°C throughout all of the experiments.

Figure 2 shows a photograph of the load frame with a sample mounted in the moiré interferometer and imaging system. The experiments employed two personal computers, one each for the data acquisition and imaging systems. Load, deflection and extension measurements were digitized to 16 bits and recorded using a conventional data acquisition system at 50 Hz. Calibration for all sensors was performed to insure accurate measurements.

Full-field Measurements

The interferometer used for these experiments was custom built with an integrated fiber optic splitter and phase shifter to provide exceptional stability and configurability [9]. Diffraction gratings were produced from holographic exposures of photographic plates. They were epoxy replicated using a method capable of producing a final grating thickness of 5–20 μm. A grating density of 300 l/mm was chosen to maximize measurement sensitivity for the anticipated range of deformations. This resulted in a fringe order sensitivity of 1.67 μm/fringe. The gratings used in this work proved extremely rugged and showed minimal physical damage and little to no degradation in signal quality for the relatively small number of loading cycles considered.

Five phase shifted images were recorded for each full-field measurement at a resolution of 1,280 × 960 pixels with 10 bit gray scale resolution. The typical field of view was on the order of 1–2 mm. Carrier fringes [4] were used to extend the range over which displacement measurements could be made. Carrier fringes are produced by changing the angles of the incident beams and provide an offset to the effective diffraction grating density. They do not increase or decrease the inherent sensitivity of moiré interferometry data, but rather change the number of fringes produced for a given deformation. By dialing in or out carrier fringes, an extended measurement range was achieved so that strain measurements could be made in both the austenite and martensite phases.

Various methods for introducing the carrier fringes and for validating the measurements produced by this method were explored. The method chosen for these experiments was confirmed to produce a repeatability better than 0.02% strain. Fringe analysis was performed manually by plotting the wrapped fringe contours and counting them edge to edge, as well as by automated methods based on the digital data. The phase shifted data provided excellent contrast for identifying fringe centers as well as resolving the slope of the wave front. The digital data superbly revealed discrete singularities and discontinuities as the phase shifting method does not obscure the data through smoothing or spatial averaging.

The gage length used for the strain calculations was kept consistent for any given series of measurements, and was usually on the order of 0.5–0.8 mm (toward the higher end of the range for the tensile measurements and the lower end of this range for the bend measurements). The choice of gage length for the full-field measurements had little significance in the strain measurements over this range for both the tensile and bend tests.

Results

Bend Tests

Figure 3 shows a sequence of images of wrapped fringes of the four-point bending for a representative sample processed according to treatment A. Figure 3(a–c) are for increasing load. Figure 3(d) is for nearing full unloading.The images clearly show that there is asymmetry in the tensile and compressive behavior material which is reflected in the off-center location of the neutral axis. This asymmetry was apparent in both samples over all of the temperature ranges tested and also occurred at stress levels below those required for phase transformation. Furthermore, detailed analysis confirmed that the axial strain distribution was linear from

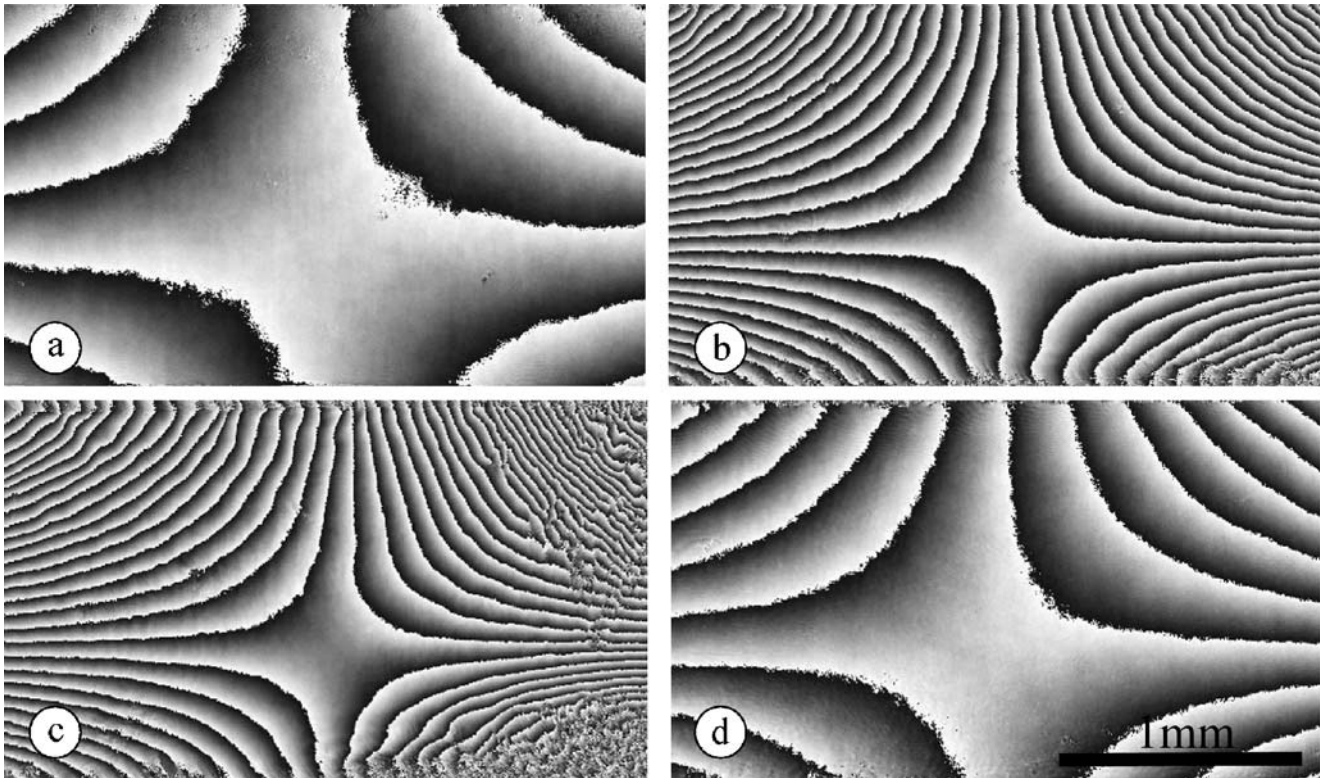

Fig. 3 Sequence of wrapped fringe patterns during loading and unloading under four-point bending for material *A*

the top edge to the bottom edge of the samples, therefore it is concluded that the asymmetry between tension and compression for these samples results from an asymmetry in the modulus of the parent phase. Figure 3(c) shows a localization band that has formed in the upper right hand corner of the image. Thus, even in pure bending, localization plays a role in the deformation behavior of superelastic nitinol.

Figures 4 and 5 show plots of load versus strain measurements for the two material heat treatments. The plots depict load versus strain measurements obtained simultaneously from the top and bottom edge of the samples for a single cycle of bending. In both cases, the slope differences in tension versus compression can be seen. In the case of treatment A shown in Fig. 4 the loading slopes exhibit the characteristic sigmoidal shape indicating the presence of substantial R-phase, as well as non-recovered strains resulting from the test being conducted slightly below this materials A_f. In contrast, the loading slopes in Fig. 5 are linear (no R-phase)

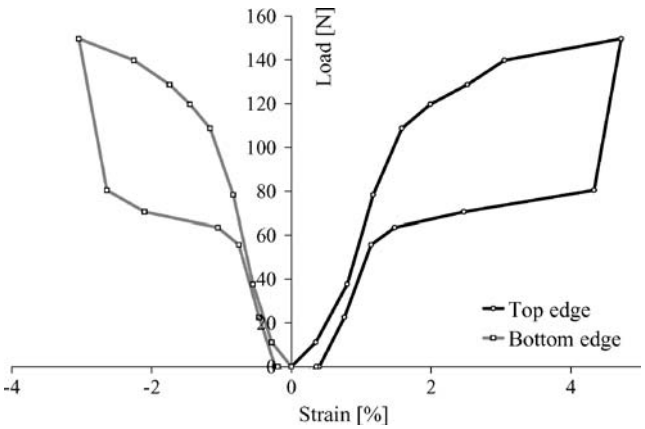

Fig. 4 Global load versus full-field strain measurements at the top and bottom edges of the sample during loading and reverse loading under four-point bend for material *A*

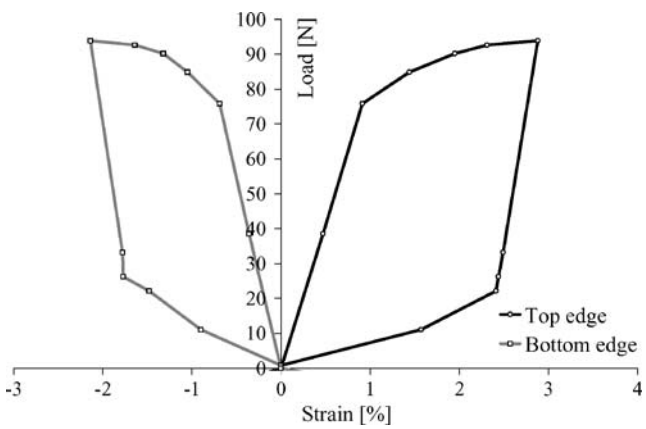

Fig. 5 Global load versus full-field strain measurements at the top and bottom edges of the sample during loading and reverse loading under four-point bend for material *B*

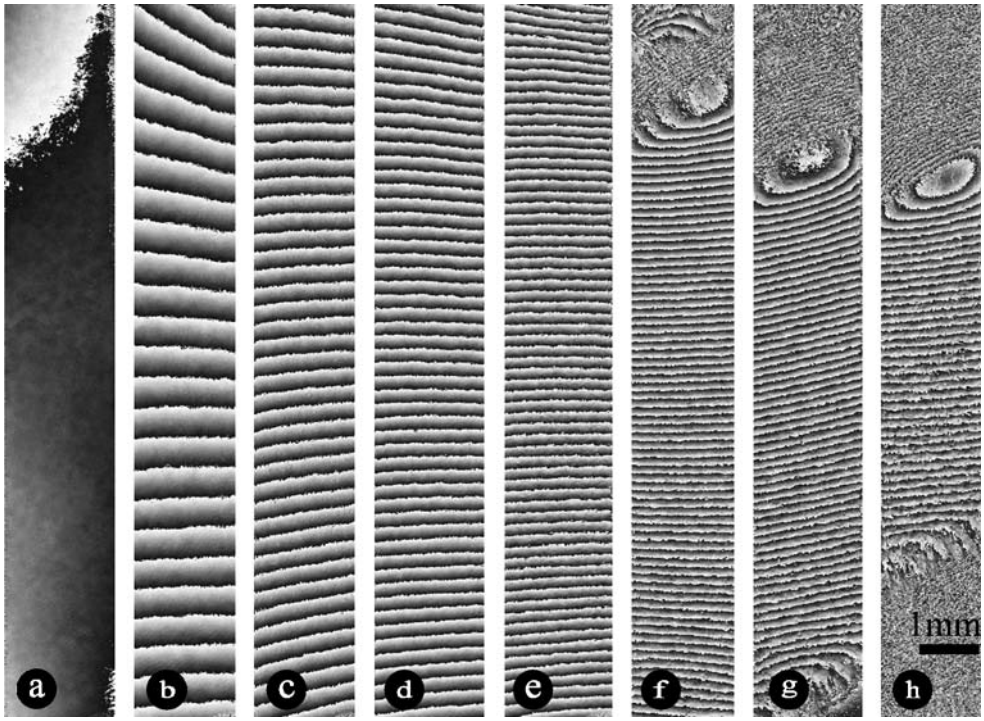

Fig. 6 Sequence of wrapped fringe patterns during the tensile loading of material *B* at a temperature above A_f

and there is no indication of unrecovered strain as this treatment B sample was tested above the A_f temperature.

Tension Tests

Uniaxial loading and unloading was performed first at temperatures above the A_f of the materials. Figure 6 shows a sequence of images of wrapped fringes of the tensile loading for a representative sample processed according to treatment B. Transformation initiates and propagates from both the top and bottom of the gage section as the loading increases and progress towards the middle of the sample. Figure 7 shows a series of optically magnified fringe patterns of the upper transformation region boundary during unloading. Strain measurements in the transformed and parent material phases are shown and qualitative differences in the fringes are readily noted for the two distinct phases. Note the fringe density in the parent phase apparently increases during the unloading shown in Fig. 7—this is a consequence of the carrier fringes added to the signal for simultaneously resolving both material phases.

Figure 8 shows the stress versus strain behavior from both the global measurements denoted by the dashed line and the full-field measurements denoted by dots

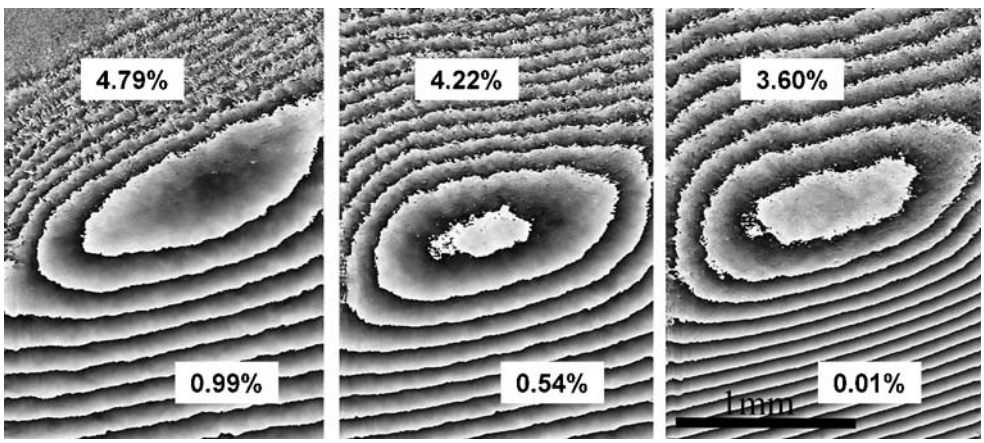

Fig. 7 Sequence of wrapped fringe patterns during the tensile unloading of material *B* at a temperature above A_f

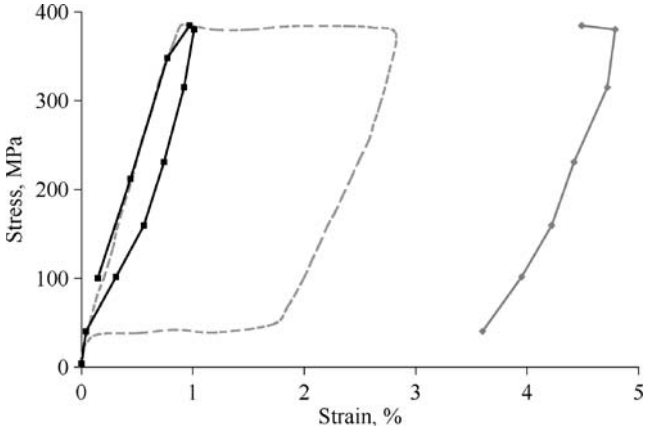

Fig. 8 Stress as a function of local strain for a typical load/unload cycle for a superelastic material above it's A_f temperature

and connected by the solid lines. Note that the full-field results show that the local strain is either in the 0 to 1% range or in the 3.5–5% range in the austenite and martensite, respectively. Strains between these two appear only in the global measurements. Measurements of parent phase and transformation zone dimensions along with the measured strain values for each can be used to compute an effective global strain estimate. The results of these calculations agree well with the global strain measurement.

Shape Memory and Thermal Recovery

After loading and unloading at a temperature above A_f, the sample temperature was raised well above A_f and then slowly lowered to the desired test temperature to insure an initial fully austenitic state. The sample was then cooled to −18°C while unconstrained. Figure 9 shows the fringe pattern (top) for the sample with treatment B at −18°C. A small two-way shape memory strain is evident as a concentration of fringes on the right hand side of the figure. Detailed analysis revealed the magnitude of this strain to be 0.37% while a small negative strain of 0.048% throughout the bulk of the sample corresponded closely with the published values of the coefficient of thermal expansion for martensite. Also shown in Fig. 9 are a strain contour plot (center) and a strain value histogram (bottom). The strain value histogram plots the number of material points having each strain value for the range of values used in the strain contour plot.

No significant two-way memory strains were observed in the material with heat treatment A for the single cycle of loading and unloading above A_f during these experiments. While we do not present here a systematic study of the shape memory training and measurement of two-way shape memory structures, these results serve to demonstrate the capabilities and precision of our measurement technique.

After cooling to below −18°C, samples of both heat treatments were loaded and unloaded in tension. In the case of the sample with treatment A, localization occurred at one end of the sample. No significant localization was observed for samples with treatment B, although localization did occur in these samples at temperatures above A_f. After the samples were unloaded, they were allowed to warm to room temperature under a controlled rate of approximately 2°/min. Figure 10 shows a series of fringe patterns for the typical free recovery of a uniaxial test sample for Treatment A. Between −18 and −2°C the localized region decreased

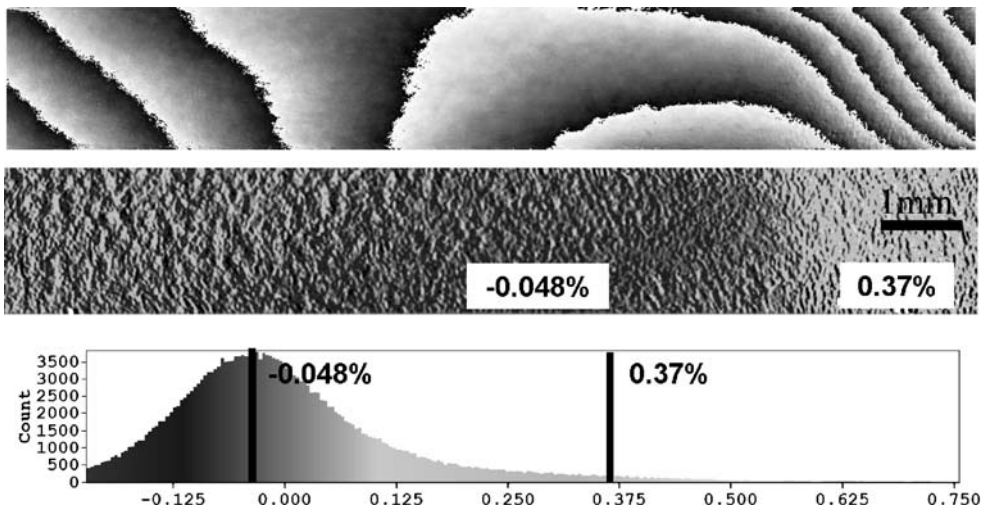

Fig. 9 Wrapped fringe pattern (*top*), strain contour plot (*center*) and strain value histogram (*bottom*) demonstrating the measurement of two-way shape and coeficient of thermal expansion for a sample with treatment *B*

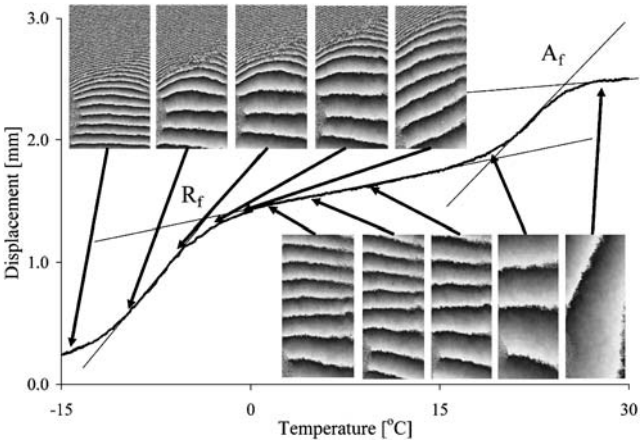

Fig. 10 Sequence of wrapped fringe patterns showing the strain recovery when a deformed sample is gradually warmed to above it's A_f temperature

slightly in size while the remainder of the sample experienced a gradual decrease in strain. Between −2 and 0.6°C the localized region quickly disappeared while the gradual strain decrease continued until the sample was retuned to above its A_f temperature.

Component Scale Measurements

Component scale measurements were made on a typical nitinol stent strut pair. The width of the struts was nominally 300 μm and the sample was shape set flat and polished to receive a diffraction grating. The sample was loaded by deforming the struts and imposing a fixed spacing between them to simulate uniform radial compression loading of 10 and 20% from the original expanded diameter. Figure 11 shows three fringe patterns corresponding to 0 load, 10 and 20% radial compression. In Fig. 11 maximum tensile strains are associated with the outer edge of the sample while peak compressive strains are located along the inner edge of the apex radius. Evidence of discontinuities appear in the fringe pattern along the outer and inner radii for the higher loading.

The application of this technique to medical components poses a significant challenge as out of plane motion and torsion can drastically degrade image quality and complicate interferometric measurements. With careful preparation and fixturing, these can be minimized, but ultimately are a limitation of the system.

Discussion

The technique of phase shifted moiré is shown here to provide accurate and reliable measurements of strain in both the parent and transformed phases of nitinol under tensile and four-point bending with large deformations. The utility of such measurement results depends on the practical measurement range and sensitivity of the measurement system which in turn depends on the quality of the fringe patterns and ultimately the quality of the replicated diffraction grating.

Fabrication of the test samples from seamless drawn tubing was chosen because of the importance of tubing to medical device applications and because processing is known to affect the behavior of nitinol. Equivalent thermomechanical processing [10] can be used to reproduce the desired material response from samples scaled to different physical dimensions. By utilizing samples produced from tubing, we have demonstrated a technique that has great utility for medical devices and their applications.

Our current results also confirm that localization occurs in samples tested under four-point bending. The degree and uniformity of the localization is markedly different from that produced in tension, most likely a result of the more controlled strain state produced in bending. This is consistent with our previous results from tests done on CT samples [5, 6]

The samples treated according to treatment A required higher loads to induce transformation than the samples treated according to treatment B. They also appeared stiffer in loading and exhibited more dramatic localization effects. Although not directly apparent in the global test results, the presence of the R-phase contributed significantly to the difference observed in the transformation strain behavior of the two treatments.

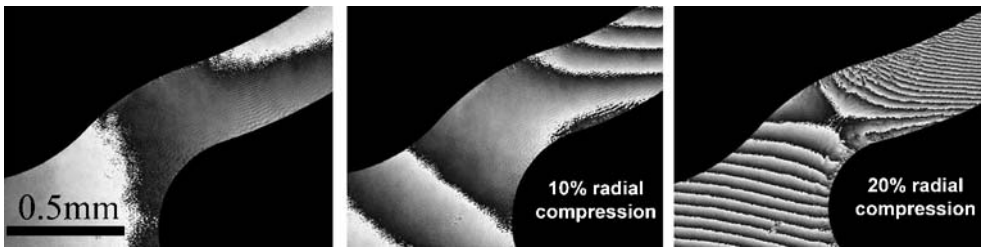

Fig. 11 Series of wrapped fringe patterns for a typical nitinol stent strut pair loaded in simulated radial compression

Conclusions

A real time, full field technique for directly measuring displacements and computing strains has been demonstrated for uniaxial tensile and four point bend loading of a nitinol coupon sample.

The novel sample geometry permits detailed studies of the differences between material with different processing histories over a wide range of temperature and loading conditions. Uniaxial tensile tests at temperatures above A_f clearly reveal the multiphase nature of the material with discrete strain values associated with each phase. Comparisons were made to global measurements of strain to highlight the need for the correct interpretation and use of such measurements for calibrating material models describing nitinol.

Different behaviors were observed for the two material heat treatments when the samples were deformed at −18°C, with the treatment A samples showing a more complicated two-step reverse transformation process. Quantification of two-way shape memory strain and determination of the coefficient of thermal expansion demonstrate the sensitivity of the measurement technique. Finally, the technique was applied to a typical nitinol implantable medical component where tension/compression asymmetry as well as phase boundary localization was observed.

Acknowledgements The authors would like to gratefully acknowledge the contributions of Randy Lloyd and Nate Stevens from the Idaho National Laboratory, Frank Scerzenie of Special Metals, and Mark Will at EDM Tek. The authors would also like to thank Alan Pelton at NDC and Brent Beuscher for helpful discussions.

References

1. Miyazaki S, Otsuka K (1989) Development of shape memory alloys. ISU Int 29(5):353–377.
2. Pelton AR, DiCello J, Miyazaki S (2001) Optimization of processing and properties of medical-grade nitinol wire. In: Russell SM, Pelton AR (eds) SMST-2000: Proceedings of the international conference on shape memory and superelastic technologies. Pacific Grove, California, International Organization on SMST, 2001, pp 361–374.
3. Sczerzenie F, Gupta S (2003) The effect of alloy formulation on the phase transformaion temperature range of NiTi shape memory alloys. In: Proceedings of the international conference on superelastic and shape memory technologies. Pacific Grove, California, International Organization on SMST, 2003, pp 15–22.
4. Post D, Han B, Ifju P (1994) High sensitivity Moiré. Springer, Berlin Heidelberg New York.
5. Labossiere PE, Perry KE (2003) The effects of notches and grain size on transformations in nitinol. In: Proceedings of the international conference on superelastic and shape memory technologies. Pacific Grove, California, International Organization on SMST, 2003.
6. Perry KE, Labossiere PE (2004) Phase transformations in nitinol and challenges for numerical modelling. In: Medical device materials II, ASM International, pp 131–134.
7. Perry Jr. KE, McKelvie J (1992) A comparison of phase-shifting and Fourier methods in the analysis of discontinuous fringe patterns. Opts Lasers Eng 19(4–5). (special issue on fringe analysis)
8. Perry KE, Labossiere PE, Steffler ES Thermoelastic transformation behavior of nitinol. American Society of Testing and Materials, JAI 9040/STP 1481. (accepted for publication)
9. Deason VA, Ward MB (1989) A compact portable difraction moiré inerferometer. In: Laser interferometry: quantitative analysis of interferograms, vol. 1162, SPIE, Bellingham, Washington, pp 26–35
10. Kugler C, Matson D, Perry KE (2001) Non-zero mean fatigue test protocol for NiTi. In: Russell SM, Pelton AR (eds) SMST-2000: Proceedings of the international conference on shape memory and superelastic technologies. Pacific Grove, California: international organization on SMST, 2001, pp 409–417.